Annals of Botany **122**: 151–164, 2018
doi: 10.1093/aob/mcy049, available online at www.academic.oup.com/aob

ANNALS OF BOTANY
Founded 1887

Gain-of-function mutation of *AtDICE1*, encoding a putative endoplasmic reticulum-localized membrane protein, causes defects in anisotropic cell elongation by disturbing cell wall integrity in Arabidopsis

Phi-Yen Le[1], Hyung-Woo Jeon[1], Min-Ha Kim[1], Eung-Jun Park[2], Hyoshin Lee[2], Indeok Hwang[3], Kyung-Hwan Han[3] and Jae-Heung Ko[1]*

[1]Department of Plant & Environmental New Resources, Kyung Hee University, Yongin 446–701, Republic of Korea, [2]Division of Forest Biotechnology, Korea Forest Research Institute, Suwon 441–847, Republic of Korea and [3]Department of Horticulture and Department of Forestry, Michigan State University, East Lansing, MI 48824, USA
**For correspondence. E-mail: jhko@khu.ac.kr*

Received: 14 December 2017 Returned for revision: 20 February 2018 Editorial decision: 13 March 2018 Accepted: 15 March 2018
Published electronically 6 April 2018

• **Background and Aims** Anisotropic cell elongation depends on cell wall relaxation and cellulose microfibril arrangement. The aim of this study was to characterize the molecular function of *AtDICE1* encoding a novel transmembrane protein involved in anisotropic cell elongation in Arabidopsis.
• **Methods** Phenotypic characterizations of transgenic Arabidopsis plants mis-regulating *AtDICE1* expression with different pharmacological treatments were made, and biochemical, cell biological and transcriptome analyses were performed.
• **Key Results** Upregulation of *AtDICE1* in Arabidopsis (35S::AtDICE1) resulted in severe dwarfism, probably caused by defects in anisotropic cell elongation. Epidermal cell swelling was evident in all tissues, and abnormal secondary wall thickenings were observed in pith cells of stems. These phenotypes were reproduced not only by inducible expression of *AtDICE1* but also by overexpression of its poplar homologue in Arabidopsis. RNA interference suppression lines of *AtDICE1* resulted in no observable phenotypic changes. Interestingly, wild-type plants treated with isoxaben, a cellulose biosynthesis inhibitor, phenocopied the 35S::AtDICE1 plants, suggesting that cellulose biosynthesis was compromised in the 35S::AtDICE1 plants. Indeed, disturbed cortical microtubule arrangements in 35S::AtDICE1/GFP-TuA6 plants were observed, and the cellulose content was significantly reduced in 35S::AtDICE1 plants. A promoter::GUS analysis showed that *AtDICE1* is mainly expressed in vascular tissue, and transient expression of GFP:AtDICE1 in tobacco suggests that AtDICE1 is probably localized in the endoplasmic reticulum (ER). In addition, the external N-terminal conserved domain of AtDICE1 was found to be necessary for AtDICE1 function. Whole transcriptome analyses of 35S::AtDICE1 revealed that many genes involved in cell wall modification and stress/defence responses were mis-regulated.
• **Conclusions** AtDICE1, a novel ER-localized transmembrane protein, may contribute to anisotropic cell elongation in the formation of vascular tissue by affecting cellulose biosynthesis.

Key words: Arabidopsis, anisotropic cell elongation, cellulose biosynthesis, cell wall integrity, endoplasmic reticulum, isoxaben, poplar, secondary wall thickening, vascular tissue formation.

INTRODUCTION

Cell elongation is a fundamental process for optimal growth and development of plants by directing proper cell morphology. Cell elongation is initiated by vacuolar turgor pressure and limited by a strong but flexible cell wall that permits directional cell elongation. Plant cell walls are essential not only for protecting cells against external stresses but also the cell elongation process (Baskin, 2005). The cell wall is composed mainly of polysaccharides (e.g. cellulose, hemicelluloses and pectins) interwoven among a relatively small amount of highly glycosylated protein (Somerville *et al.*, 2004; Carpita, 2011). The strongest component in the cell wall is a network of cellulose microfibrils. While cellulose microfibrils are synthesized by cellulose synthase (CesA) complexes (CSCs) at the plasma membrane (PM) and are extruded directly into the cell wall (Geisler *et al.*, 2008; McFarlane *et al.*, 2014), other polysaccharides are synthesized in the endoplasmic reticulum (ER) or Golgi and delivered to the cell wall through the intracellular secretory pathway (Gibeaut and Carpita, 1994). CesA subunits are synthesized in the ER, and CSC rosettes are assembled in the Golgi, transported via the trans-Golgi network (TGN) and inserted into the PM through cortical microtubule-assisted vesicle trafficking (Paredez *et al.*, 2006; McFarlane *et al.*, 2014; Zhang *et al.*, 2016).

Cellulose microfibrils, as load-bearing components of the cell wall, are important in controlling anisotropic cell elongation in plants. Cellulose microfibrils are aligned perpendicular to the axis of elongation, thus forming a spring-like structure that reinforces the cell crosswise and favours longitudinal expansion in most growing cells (Baskin, 2005; Lei *et al.*, 2014). Furthermore,

because the newly synthesized cellulose microfibrils are aligned by the cortical microtubules through microtubule–CSC interacting proteins, such as CSI1/POM2, CSI3 and CC, it has been suggested that the shape of plant cells is determined by the orientation of cortical microtubules (Green, 1962; Bringmann *et al.*, 2012; Endler *et al.*, 2015). Thus, perturbation of either microtubules or cellulose microfibril organization leads to defects in cell elongation (Fagard *et al.*, 2000; Lane *et al.*, 2001; Schindelman *et al.*, 2001; Pagant *et al.*, 2002; Caño-Delgado *et al.*, 2003; Somerville, 2006; Wang *et al.*, 2006). The dwarf phenotype of cellulose-deficient mutants is therefore commonly interpreted as resulting from the loss of anisotropic cell elongation by weakened cell walls.

Many genes involved in either cell expansion or cellulose biosynthesis have been identified through genetic screening and subsequent cloning. For example, mutation of *RSW1*/*CesA1*, *RSW5*/*CesA3*, *QUILL*/*PROCUSTE*/*CesA6*, *POM-POM1*/*CHITINASE LIKE1* (*POM1*/*CTL1*), *KORRIGAN*/*LION'S TAIL1*/*RADIALLY SWOLLEN2* (*KOR*/*LIT*/*RSW2*), *COBRA* and *KOBITO*/*ELONGATION DEFECTIVE1* (*KOB1*/*ELD1*) was associated with epidermal cell swelling, restricted elongation of root and hypocotyl, and reduced cell wall cellulose content (Hauser *et al.*, 1995; Arioli *et al.*, 1998; Nicol *et al.*, 1998; Fagard *et al.*, 2000; Lane *et al.*, 2001; Schindelman *et al.*, 2001; Pagant *et al.*, 2002; Wang *et al.*, 2006). During cell expansion, the integrity of the cell wall is vital. Once the integrity of the cell wall is disrupted, a series of compensatory reactions, such as ectopic accumulation of lignin and callose, modification of cell wall composition, and enhanced stress/defence responses, follow. For example, mutations or treatment with chemical inhibitors of cellulose biosynthesis lead to ectopic lignification and/or callose deposition, and change the composition of the cell wall matrix (Desprez *et al.*, 2002; Pagant *et al.*, 2002). In both *eli1* (*ECTOPIC LIGNIFICATION1*) (Caño-Delgado *et al.*, 2000) and *cev1* (*CONSTITUTIVE EXPRESSION OF VSP1*) (Ellis and Turner, 2001) mutants, which were identified as different mutant alleles of a cellulose synthase gene *CesA3*, the jasmonic acid (JA) and ethylene-signalling pathways were highly activated and stress responsive genes were up-regulated. Also, *cob-5*, a loss of function mutant of *COBRA*, exhibits abnormal cell growth with a massive accumulation of stress response chemicals, such as anthocyanins and callose. Furthermore, *cob-5* over-accumulates JA and induces defence and stress-related genes coordinately (Ko *et al.*, 2006*b*). These reports suggest that plant cells initially sense biotic stresses at the level of the integrity of the cell wall (Ko *et al.*, 2006*b*; Wolf *et al.*, 2012).

In this study, we report the functional characterization of a gene named *AtDICE1* (*DEFECT IN CELL ELONGATION1*) from Arabidopsis. A gain-of-function mutation of *AtDICE1* caused severe dwarfism with defects in anisotropic cell elongation. Further anatomical, molecular, biochemical and whole transcriptome analyses suggest that AtDICE1 is a novel ER-localized transmembrane protein contributing to the proper anisotropic cell elongation process in the vascular tissue through participation in cell wall formation.

MATERIALS AND METHODS

Plant materials and growth conditions

Arabidopsis thaliana, ecotype Columbia (Col-0), was used in both the wild-type (WT) and transgenic experiments. Plants were growth on soil or on MS-agar plates [0.5× MS, 2 % sucrose, 0.8 % (w/v) agar] in a growth chamber (16-h light/8-h dark) at 23 ± 2 °C, after stratification. For the growth measurement of young seedlings, MS-agar plates were vertically orientated. For isoxaben (36138, Sigma-Aldrich, St Louis, MO, USA) treatment, isoxaben was dissolved in methanol and added to the *A. thaliana* seedling cultures to final concentrations of 1, 5 or 10 nM. Seedlings were grown in 0.5× MS medium containing 2 % (w/v) sucrose, 0.8 % (w/v) agar and isoxaben at different concentrations and observed after 7 d.

Histological analysis

The stem area located immediately above the rosette (basal level) was cross-sectioned by hand and stained with 2 % phloroglucinol/HCl or 0.05 % toluidine blue *O* for 1 min. Microtome (Leica RM2025, Leica, http://www.leica.com) sectioning after paraffin embedding was used to observe the detailed structure of hypocotyls and stems. For confocal laser scanning microscopy, a Zeiss PASCAL microscope (Jena, Germany), with a 488-nm excitation mirror, a 560-nm emission filter and a 505–530-nm emission filter, was used to record images. Image analysis was performed using laser scanning microscope PASCAL LSM version 3.0 SP3 software. For scanning electron microscopy (SEM), a tabletop microscope (Hitachi TM3000, Tokyo, Japan) was used to visualize hypocotyls from 7-d-old seedlings of WT and 35S::AtDICE1 (7-5 line) plants using the default conditions without any pretreatments.

Plasmid vector construction and generation of transgenic Arabidopsis plants

The full-length cDNA of *AtDICE1* (At2g41610) was amplified by PCR and inserted downstream of the 35S promoter in the pB2GW7 or pB7BWIWG2(II) vectors (Karimi *et al.*, 2002) using the Gateway cloning system to produce 35S::AtDICE1 or 35S::AtDICE1-RNAi constructs, respectively. The N-terminal deletion fragment of *AtDICE1* (ΔNT-AtDICE1) was amplified by PCR using the 35S::AtDICE1 construct as a template and inserted downstream of the 35S promoter in the pB2GW7 vector to produce the 35S::ΔNT-AtDICE1 construct. For the *AtDICE1* promoter::GUS construct, the 1.0-kb *Xba*I/*Bam*HI genomic fragment flanking the 5′ end of the AtDICE1 coding sequence was amplified using genomic DNA extracted from Arabidopsis leaf tissue as template, and subcloned into the pCB308 vector (Xiang *et al.*, 1999). To construct the 35S::GFP:AtDICE1 plasmid, the Gateway destination vector pEarleyGate103 was used to translationally fused GFP:AtDICE1. All the vector constructs produced were verified by DNA sequencing and introduced into *Agrobacterium tumefaciens* (C58), which was used to transform Arabidopsis (Col-0) or the GFP-TuA6 background using the floral-dip method described by Clough and Bent (1998).

Extraction of alcohol-insoluble cell wall residue

Stem tissues (5 cm from rosette level) from 60-d-old WT and 35S::AtDICE1 plants were ground to a fine powder. The

ground material (approx. 1 g) was washed in 15 mL of 70 % ethanol and heated for 15 min at 70 °C to inactivate endogenous enzymes and remove the cell contents. Samples were centrifuged for 10 min at 4000 *g*, and the pellets were washed twice with 100 % ethanol and once with 100 % acetone. The remaining pellet was considered to be the alcohol-insoluble cell wall residue (AIR) and was dried at 70 °C.

Analysis of cell wall monosaccharide composition

Cell wall sugars (as alditol acetates) were determined using the procedure reported by Hoebler *et al.* (1989). Briefly, AIRs (3 mg) were incubated with 70 % sulfuric acid at room temperature for 30 min, followed by the addition of inositol as the internal standard and dilution with water to a final concentration of 6 % sulfuric acid. After heating for 120 min at 105 °C, the solution was treated with 25 % ammonium solution. After reduction with sodium borohydride in dimethyl sulfoxide, the solution was heated for 90 min at 40 °C, followed by sequential treatment with glacial acetic acid, acetic anhydride, 1-methylimidazole, dichloromethane and water. The organic layer containing the alditol acetates of the hydrolysed cell wall sugars was washed three times with water, and sugars were analysed on a gas–liquid chromatograph (model 6890; Hewlett-Packard, http://www.hp.com) equipped with a 30 m × 0.25 mm (i.d.) silica capillary column DB 225 (Alltech Associates Inc., Deerfield, IL, USA).

Statistical analysis

Data were analysed with a two-tailed, unpaired *t*-test by using GRAPHPAD PRISM 7.03 (Graphpad Software, San Diego, CA, USA). *P*-values of <0.05 were considered significant.

Histochemical GUS staining

Histochemical GUS staining of transgenic plants was performed as described by Jefferson *et al.* (1987) with slight modifications as described by Nguyen *et al.* (2016). Briefly, samples were incubated at 37 °C for 18–24 h in GUS reaction buffer and visualized after removing chlorophyll by rinsing with 70 % ethanol.

Intracellular localization of AtDICE1

Each 35S::GFP and 35S::GFP:AtDICE1 construct was introduced into *Agrobacterium tumefaciens* (strain C58) by the freeze–thaw method (Höfgen and Willmitzer, 1988). Transient expression in *Nicotiana benthamiana* leaf epidermal cells was determined by the agroinfiltration method (Di Sansebastiano *et al.*, 2004). The *N. benthamiana* leaves were further grown for 12 h, and the fluorescence was observed using a Zeiss PASCAL confocal laser scanning microscope as described above.

RNA extraction and semi-quantitative RT-PCR analysis

Total RNAs were extracted using Trizol reagent (Gibco-BRL, http://www.invitrogen.com) according to the manufacturer's instructions. Total RNAs were reverse transcribed using Superscript II reverse transcriptase (Invitrogen) in 20-µL reactions. Semi-quantitative reverse transcriptase PCR (RT-PCR) was carried out using 1 µΛ of the reaction products as a template. Amplified DNA fragments were separated on a 1 % agarose gel and stained with ethidium bromide. The primers used for RT-PCR analysis are shown in Supplementary Data Table S3.

Whole transcriptome microarray analysis

Total RNAs were isolated from 7-d-old seedlings of 35S::AtDICE1 (7-5, 10-1, 11-6) and WT grown on MS agar plates. An Agilent Bioanalyzer (Agilent, Santa Clara, CA, USA) was used to check RNA quality. Nucleic acid labelling was performed according to the manufacturer's recommended procedures for single-colour arrays. Labelled RNA was hybridized to Agilent 4x44K Arabidopsis Gene Expression (V4) Microarrays (Agilent G2519F-021169). Arrays were scanned with an Agilent G2565B Array Scanner, and images were analysed using the Feature Extractor v9.5 default protocol GE1-v5_95_Feb07. The resulting hybridization intensity values (i.e. signal intensity) of each spot reflect the abundance of a given mRNA relative to the total mRNA population and were used in all subsequent analyses. All data normalization and selection of genes showing fold-changes were performed using GeneSpringGX 7.3.1 (Agilent). Genes were filtered by removing flag-out genes in each experiment. Intensity-dependent normalization [locally weighted scatterplot smoothing (LOWESS)] was performed, where the ratio was reduced to the residual of the LOWESS fit of the intensity versus ratio curve. The averages of normalized ratios were calculated by dividing the average of the normalized signal channel intensity by the average of normalized control channel intensity. Differentially expressed genes were identified using the Single *t*-test, which assumes unequal variances between groups. The criterion for significant genes was $P < 0.05$. The raw microarray data were deposited in the Gene Expression Omnibus database together with details of the protocol.

RESULTS

Overexpression of AtDICE1 *results in a severe dwarf phenotype*

Previously, using a global comparative transcriptome analysis, we found a gene network regulating secondary xylem development in Arabidopsis (Ko *et al.*, 2006*a*). Among the genes in this network, we were interested in a completely unknown gene locus, At2g41610, which we named *AtDICE1*. *AtDICE1* is specifically expressed in vascular tissues or cells (Supplementary Data Fig. S1) and the Potri.014G108300 gene (named as *PtrDICE1*), the closest homologue of *AtDICE1* in poplar, is also preferentially expressed in the wood-forming tissues of poplar (Fig. S1C). Consistently, our promoter–GUS reporter analysis showed that *AtDICE1* promoter activity was detected mainly in the vascular tissues of cotyledon and hypocotyl, and in the roots of young seedlings as early as 2 d old (Fig. S1D). In cross-sections of stems and roots, activity of the *AtDICE1* promoter was found mainly in vascular bundles, especially in cambium and/or xylem parenchyma cells (Fig. S1E). Further sequence

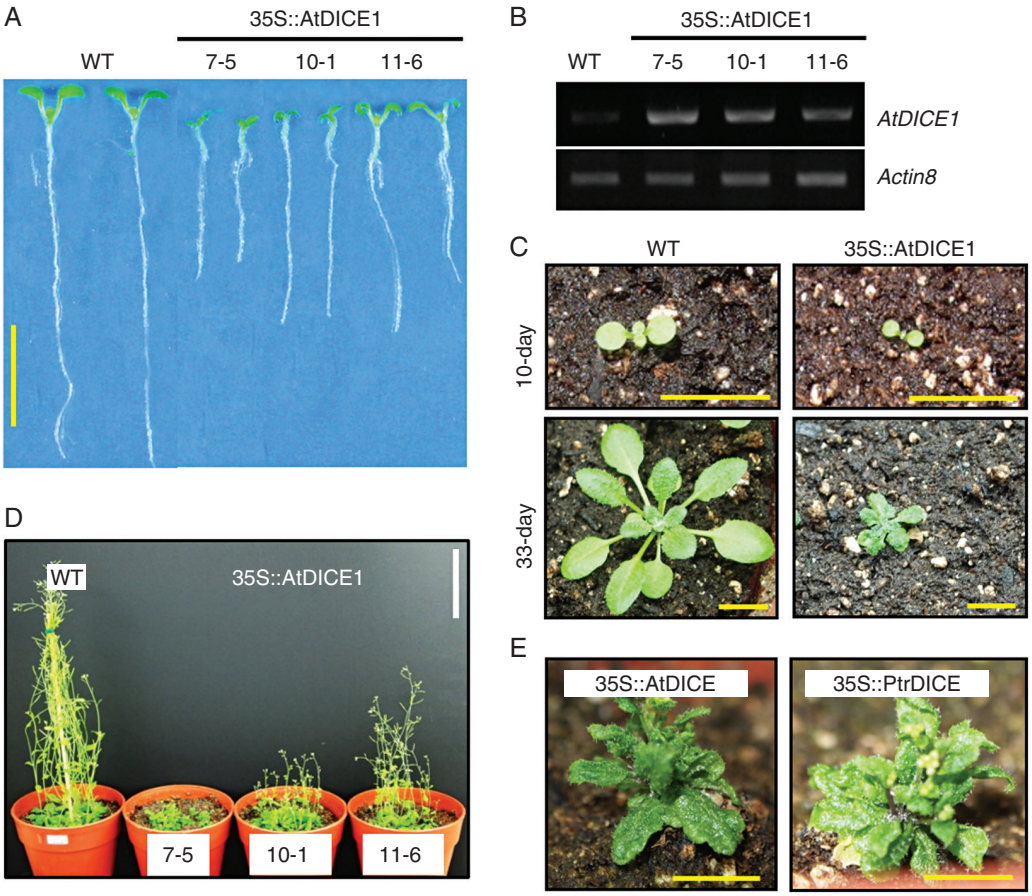

FIG. 1. Gain-of-function mutation of *AtDICE1* resulted in a severe dwarfing phenotype. (A) Seven-day-old seedlings of wild-type (WT) and 35S::AtDICE1 plants. (B) Semi-quantitative RT-PCR analysis for *AtDICE1* transcript accumulation in each of three T3 homozygote 35S::AtDICE1 plants. *Actin8* was used as a control. (C) Growth features of 35S::AtDICE1 (line 7-5) and WT plants on soil at 10 d (upper) and 33 d (lower). (D) Forty-day-old WT and 35S::AtDICE1 (7-5) plants grown in pots. (E) Forty-day-old 35S::AtDICE1 (7-5) (left) and 35S::PtrDICE1 (right) plants. Scale bars represent 1 cm, except 10 cm in D.

analysis identified that *AtDICE1* is a plant-specific and transmembrane protein (Fig. S2). Both TMHMM (http://www.cbs.dtu.dk/services/TMHMM-2.0/) and SOSUI (http://bp.nuap.nagoya-u.ac.jp/sosui/) analyses predicted that *AtDICE1* has seven transmembrane domains with the N-terminus outside and C-terminus inside (Fig. S2B, C). Interestingly, the putative external N-terminal motif is highly conserved in all plant species examined (Fig. S2A).

To characterize the molecular function of *AtDICE1*, we first generated gain-of-function transgenic Arabidopsis plants by overexpressing *AtDICE1* under control of the cauliflower mosaic virus (CaMV) 35S promoter (i.e. 35S::AtDICE1 plants). This was done because T-DNA knock-out mutants were unfortunately not available. A total of 26 T1 transgenic plants were examined and we found that most of them were dwarfed compared to WT Arabidopsis plants (data not shown). To perform additional detailed analyses, three T3 homozygote transgenic plants (i.e. 7-5, 10-1 and 11-6 lines of 35S::AtDICE1) based on phenotypic severity were selected (Fig. 1). The dwarfing phenotypes of 35S::AtDICE1 plants were evident not only in young seedlings but also at the adult stage (Fig. 1; Table S1). Furthermore, the degree of dwarfing was consistent with the expression levels of the *AtDICE1* gene (Fig. 1B). In adult plants, 35S::AtDICE1 plants showed extremely small rosette leaves, very short inflorescence stems, small flowers and reduced apical dominances (Figs 1C, D and S3). Furthermore, overexpression of *PtrDICE1* reproduced almost the identical phenotype observed in 35S::AtDICE1 plants (Fig. 1E). This result suggests that *PtrDICE1* is orthologous to *AtDICE1*.

We produced RNA interference (RNAi) suppression lines of *AtDICE1* (i.e. 35S::AtDICE1-RNAi) to analyse the loss-of-function phenotype (Fig. S4). Among a total of seven independent T3 homozygous lines, two of them (7-1, 12-1) showed significantly decreased expression of *AtDICE1* (Fig. S4A). However, we were unable to observe any significant alterations in phenotype in seedlings or adult plants (Fig. S4B, C).

35S::AtDICE1 plants exhibit defects in anisotropic cell elongation

In young seedlings of 35S::AtDICE1 plants, epidermal cell swelling is evident in both hypocotyls and cotyledons; this was never seen in WT seedlings (Fig. 2). Analysis of a cross-section of hypocotyls from 7-d-old seedlings revealed that the cell swelling was found not only in epidermal cells but also in cells inside,

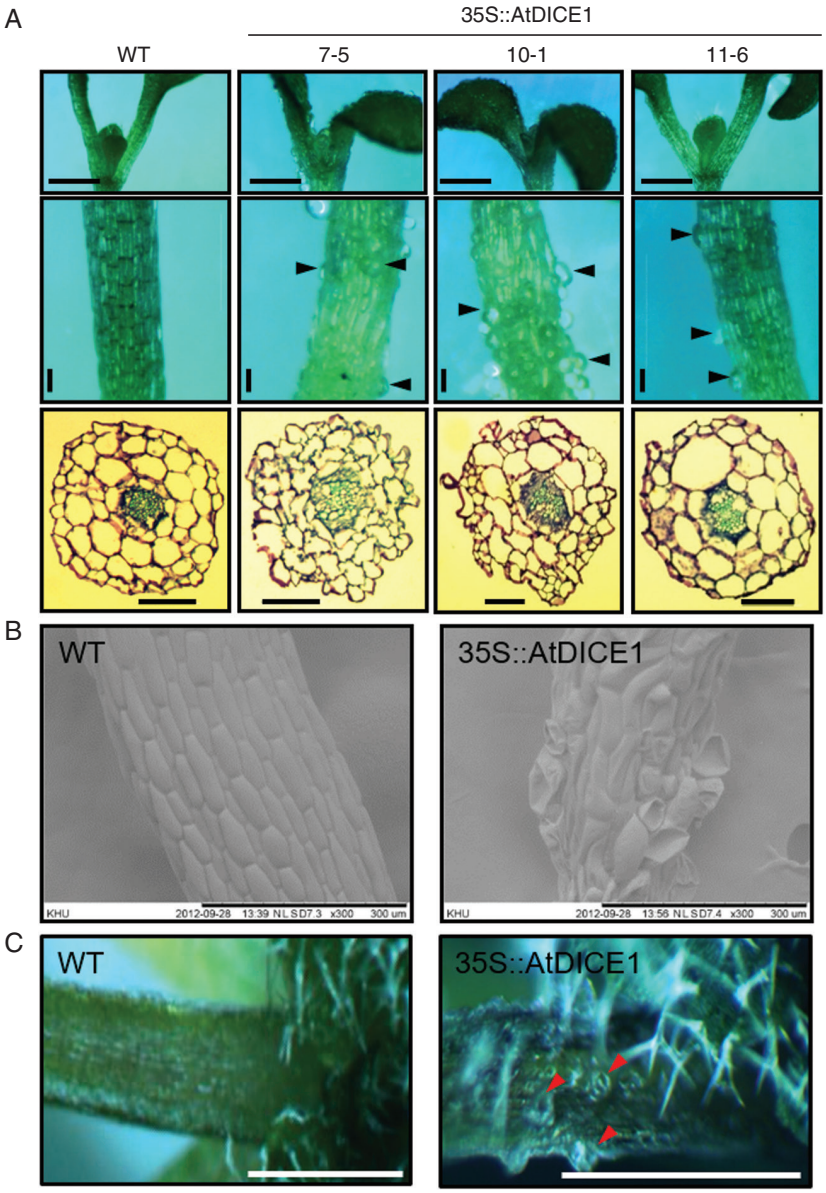

FIG. 2. 35S::AtDICE1 plants showed defects of anisotropic cell expansion. (A) Epidermal cell swelling in cotyledons (upper), hypocotyls (middle) and hypocotyl cross-sections (lower) of 7-d-old 35S::AtDICE1 seedlings compared to WT. Arrowheads indicate swollen cells. Scale bars represent 1 mm (top), 100 μm (middle and bottom). (B) Scanning electron micrographs of hypocotyls of 7-d-old plants. (C) Petioles of rosette leaves from 30-d-old plants. Arrowheads indicate swollen cells. Scale bars represent 0.5 cm.

which caused disarray of the cell arrangement in 35S::AtDICE1 plants (Fig. 2A). SEM clearly showed epidermal cell enlargements, which were distorted during the imaging process due to vacuum application (Fig. 2B). This isotropic cell expansion was found persistently in adult plants (Fig. 2C), which probably caused the severe dwarfism of 35S::AtDICE1 plants. To verify this phenotype, we produced additional transgenic Arabidopsis plants in which *AtDICE1* expression can be induced. For inducible gene expression, the Gateway Destination vector pMDC7 (Curtis and Grossniklaus, 2003) was used. This vector contains the XVE inducible promoter for 17-β-estradiol inducible expression in plants (Fig. 3). Our results clearly demonstrated that treatment with 17-β-estradiol at concentrations as low as 10 αM successfully induced *AtDICE1* expression (Fig. 3A) and resulted in epidermal cell swelling as early as in 2-d-old seedlings (Fig. 3B).

Cellulose biosynthesis is impaired in 35S::AtDICE1 plants

Perturbations in either cellulose biosynthesis or cortical microtubule arrangements are known to cause cell swelling (Fagard *et al.*, 2000; Lane *et al.*, 2001; Schindelman *et al.*, 2001; Pagant *et al.*, 2002; Caño-Delgado *et al.*, 2003; Somerville, 2006; Wang *et al.*, 2006). To test our hypothesis, isoxaben, a well-known inhibitor of cellulose biosynthesis, was applied to

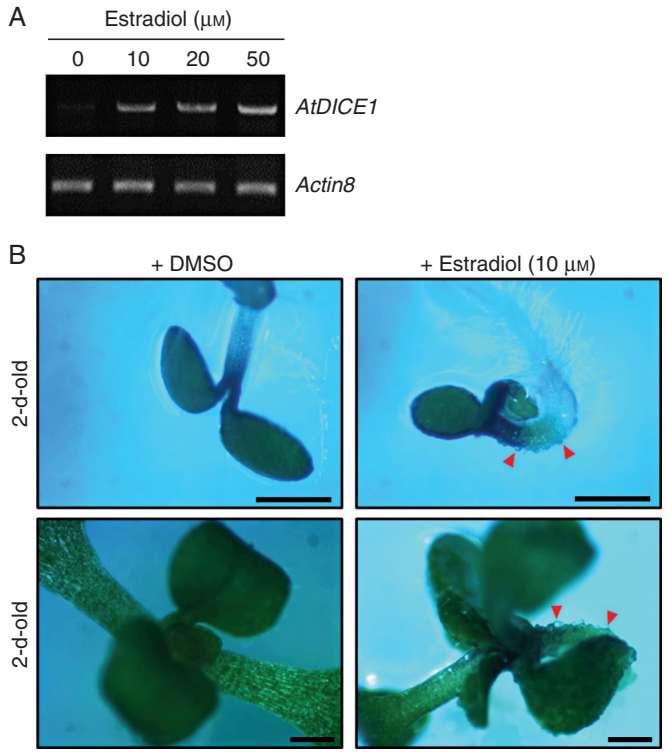

FIG. 3. Inducible expression of *AtDICE1* reproduced the cell swelling phenotype of 35S::AtDICE1 plants. (A) Semi-quantitative RT-PCR analysis performed to confirm *AtDICE1* induction by 17-β-estradiol treatment of 10-d-old seedlings of T3 homozygous AtDICE1/pMDC7 plants (line 8-4). (B) Estradiol treatment of AtDICE1/pMDC7 plants (line 8-4). AtDICE1/pMDC7 plants were grown on MS-agar plates with (+Estradiol) or without 17-β-estradiol (+DMSO). Red arrowheads indicate epidermal cell swelling. Scale bars represent 1 mm.

both WT and 35S::AtDICE1 plants. Treatment of WT plants with isoxaben successfully mimicked the epidermal cell swelling phenotype of 35S::AtDICE1 plants at concentrations as low as 5 nM (Fig. 4A). Because isoxaben treatment is known to prevent the insertion of CSCs into the PM (Paredez *et al.*, 2006; Gutierrez *et al.*, 2009), the cell swelling phenotype was probably caused by defects in cellulose biosynthesis in the cell wall.

To further confirm whether cellulose biosynthesis was affected in 35S::AtDICE1 plants, we analysed the monosaccharide composition of cell wall materials prepared from stem tissues of WT and 35S::AtDICE1 plants. To our surprise, the glucose content was significantly decreased in 35S::AtDICE1 plants (Fig. 4B). Because the AIRs of the cell wall were used in this analysis, most of the glucose content came from the degradation of cellulose. Thus, this result suggests that the cellulose content of the cell walls of 35S::AtDICE1 plants was reduced.

Next, to determine whether there were any changes in the cortical microtubule arrangement of 35S::AtDICE1 plants, we overexpressed AtDICE1 in GFP-TuA6 plants. These plants constitutively express a green fluorescent protein (GFP)-fused tubulin A6, and thus cortical microtubules can be visualized using confocal microscopy (Ueda and Matsuyama, 2000). Interestingly, we were able to observe abnormal arrangements of cortical microtubules in swollen cells from 35S::AtDICE1/GFP-TuA6 plants compared to GFP-TuA6 plants, which showed arrangements of microtubules perpendicular to the elongation direction (Fig. 4C).

AtDICE1 protein is probably localized in the ER

Our amino acid sequence analysis of *AtDICE1* suggested that AtDICE1 is a putative transmembrane protein having seven transmembrane domains (Fig. S2). To investigate the intracellular localization of AtDICE1, a transient expression analysis was performed using tobacco epidermal cells. The vector construct expressing the AtDICE1 protein fused to the C-terminus of GFP driven by the CaMV 35S promoter (35S::GFP:AtDICE1) was introduced into the leaves of tobacco using *Agrobacterium* and the epidermal cells were observed under a confocal laser microscope. As shown in Fig. 5, the fluorescent signal of GFP:AtDICE1 was observed exclusively in the reticulate tubular networks and in sheets typical of the ER in the cortical regions of cells, indicating that AtDICE1 is probably localized in the ER. The same result was obtained by using the 35S::AtDICE1:GFP construct (data not shown). By contrast, in a control experiment, the fluorescent signal of GFP alone was found in the plasma membrane, cytoplasm and nucleus of the cells (Fig. 5).

The N-terminal conserved domain is necessary for AtDICE1 function

Because AtDICE1 has a putative external N-terminal motif, which is highly conserved in the plant species examined (Fig. S2A), we attempted to determine the functional significance of the motif using deletion analysis. We generated transgenic Arabidopsis plants overexpressing an N-terminal deleted *AtDICE1* gene (35S::ΔNT-AtDICE1) (Fig. 6A, B). However, we did not observe any phenotypic changes in either the young seedlings or adult plants of the 19 independent T3 homozygous transgenic plants we examined (Fig. 6C, D). This suggests that the highly conserved N-terminal external domain of AtDICE1 might play an important role in AtDICE1 function.

Transcription phenotype of 35S::AtDICE1 plants is highly correlated with its physiological phenotype

To examine the transcription phenotype of 35S::AtDICE1 plants, a whole-transcriptome analysis was performed using total RNAs extracted from 7-d-old seedlings of three independent T3 homozygous lines of 35S::AtDICE1 (i.e. 7-5, 10-1, 11-6) and WT plants grown on MS agar plates (see Materials and Methods). Gene expression profiles were obtained using Agilent's Whole Arabidopsis Gene Expression Microarray (G2519F-021169, V4, 4x44K), which contains a total of 43 505 probe sets covering the entire Arabidopsis transcriptome (http://www.genomics.agilent.com). In the subsequent gene expression analysis, we found a total of 90 probe sets (representing 72 genes) which were significantly upregulated (three-fold as a threshold) in all three lines of 35S::AtDICE1 plants compared to WT plants. Meanwhile only 17 probe sets (representing 16 genes) were downregulated (Fig. 7A, B; Table S2).

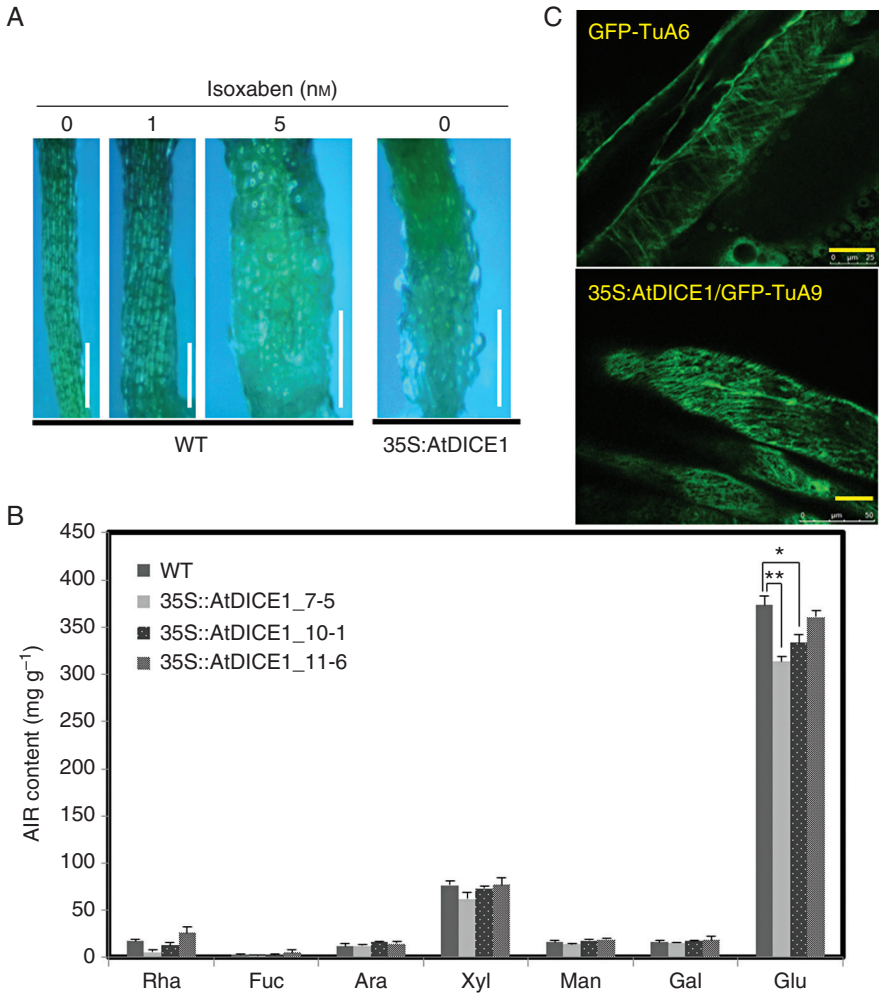

FIG. 4. 35S::AtDICE1 resulted in defects in cellulose biosynthesis. (A) Treatment with isoxaben in WT plants. Plants were grown for 7 d on MS-agar plates containing isoxaben as indicated. Scale bars represent 0.5 mm. (B) Cell wall monosaccharide composition analysis. Inflorescence stems of 60-d-old soil-grown plants were used. AIR, alcohol-insoluble residue. Neutral monosaccharides in the sulfuric acid-soluble fraction were determined by quantification of their corresponding alditol acetates by gas chromatography. Rha, rhamnose; Fuc, fucose; Ara, arabinose; Xyl, xylose; Man, mannose; Gal, galactose; Glu, glucose. Error bars indicate s.e. using triplicate experiments (*$P < 0.05$; **$P < 0.01$, unpaired *t*-test). (C) Observation of cortical microtubule arrangement by confocal laser microscopy. Cortical microtubules were visualized in normal cells from GFP-TuA6 plants (upper) and swollen cells from 35S::AtDICE1/GFP-TuA6 plants (lower). Scale bars indicate 25 αμ.

To gain functional insight into the 72 upregulated genes in 35S::AtDICE1, we performed Gene Ontology (GO) analyses (Fig. 7C, D). In the REVIGO (http://revigo.irb.hr) analysis, which provides a visual summary of the long list of GO terms as a scatterplot by removing redundant GO terms, the responses to stress, response to organic substance (e.g. JA) and defence response categories plotted most clearly (Fig. 7C). In addition, using the Classification SuperViewer tool (http://bar.utoronto.ca/ntools/cgi-bin/ntools_classification_superviewer.cgi), genes related to the abiotic/biotic stimulus, response to stress and cell wall categories were found to be over-represented (Fig. 7D). Accordingly, more than half of the 72 upregulated genes (37 genes, 51.4 %) were involved in the stress and/or defence mechanisms (Table 1). In addition, many cell wall formation and modification-related genes were significantly upregulated, which probably reflects the defects in the cell elongation phenotype of 35S::AtDICE1 plants (Fig. 7D and Table 1). These results clearly show that the transcription phenotype of 35S::AtDICE1 plants is highly correlated with its physiological phenotype.

To verify the microarray results, we performed a semi-quantitative RT-PCR analysis of 15 selected genes, including six that were upregulated, four that were downregulated and five that had no significant changes in gene expression in 35S::AtDICE1 plants. The band intensities of the PCR products were quite comparable to the microarray data (Fig. S5).

Abnormal secondary wall thickenings in pith cells of the inflorescent stem in 35S::AtDICE1 plants

Because the growth of inflorescent stems in 35S::AtDICE1 plants was severely inhibited and the surface of the stems was bumpy, the anatomy of the inflorescent stems of 35S::AtDICE1and WT plants was examined using microtome sectioning. Surprisingly, we found abnormal secondary

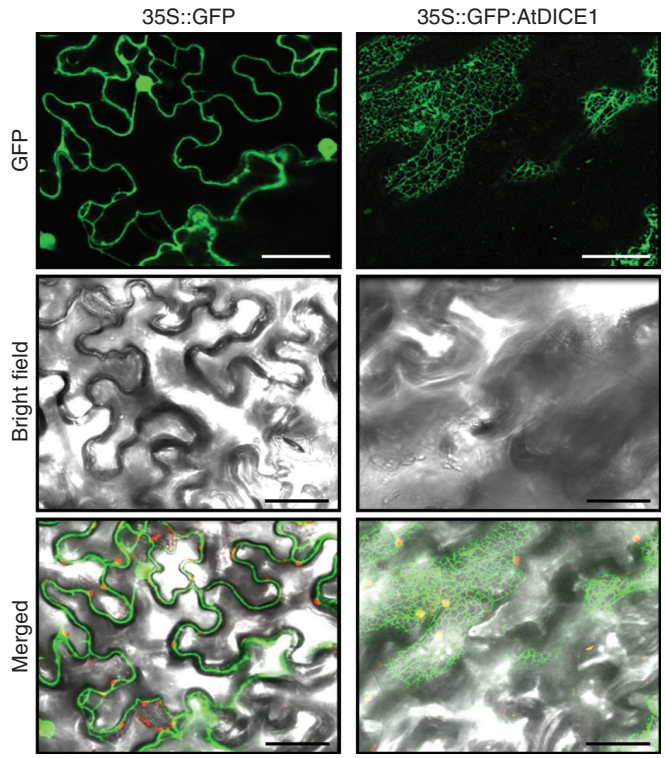

FIG. 5. Intracellular localization of the AtDICE1 protein. Intracellular localization of either GFP alone (left) or GFP:AtDICE1 (right) driven by the 35S promoter was observed by confocal imaging of transiently transformed tobacco epidermal leaf cells. Single confocal optical sections visualizing images of GFP fluorescence (500–520 nm) were photographed using dark field (upper) and bright field (middle) and then merged (lower). Scale bars represent 50 αμ.

wall thickenings in the pith cells of 35S::AtDICE1 plants in addition to the epidermal cell swelling/enlargements (Fig. 8). This phenotype was also observed in the stem sections of 35S::PtrDICE1 plants (Fig. S7). Cross-sections along the stem length indicate that these abnormal secondary wall thickenings are regional or sporadic (Fig. S7B). Interestingly, this result is reminiscent of the *eli1* mutant, which has defects in cell expansion due to mutation of the *CesA3* gene (Caño-Delgado *et al.*, 2000, 2003).

DISCUSSION

Precise regulation of cell expansion is essential for cellular morphogenesis and differentiation and consequently directs typical plant growth and development. It is well known that cellulose microfibrils strengthen cell walls and define the direction of anisotropic cell growth (Cosgrove, 2005; Lloyd and Chan, 2006). In this report, we attempted to characterize a gene locus, *AtDICE1*, which encodes a novel transmembrane protein probably localized to the ER.

Upregulation of AtDICE1 *caused abnormal cell expansion*

Upregulation of *AtDICE1* caused severe growth and developmental defects at the whole plant level (Figs 1, 2 and S3, Table S1). The prominent cell swelling phenotype, caused by defects in anisotropic cell expansion, probably accounted for the dwarf phenotype of 35S::AtDICE1 plants (Figs 2 and 3). This phenotypic consequence was reproduced by overexpression of *PtrDICE1*, a poplar homologue of AtDICE1 (Fig. 1E) and was further verified by inducible expression of *AtDICE1* which resulted in a clear phenotype as early as in 2-d-old Arabidopsis seedlings (Fig. 3).

We hypothesized that the cell swelling phenotype of 35S::AtDICE1 plants may result from alterations in cell wall integrity, especially the decrease in cellulose content estimated from our cell wall monosaccharide analysis (Fig. 4). This is further supported by the following results: (1) treatment with isoxaben, a well-known cellulose synthase inhibitor, mimicked the cell swelling phenotype of 35S::AtDICE1 plants in WT plants (Fig. 4A), and (2) cortical microtubule arrangements, which direct proper cellulose deposition in cell walls via an association with CesA interacting1/CSI1 (Paredez *et al.*, 2006; Bringmann *et al.*, 2012; Li *et al.*, 2012), were severely altered in 35S::AtDICE1/GFP-TuA6 plants (Fig. 4C). Previously, loss-of-function mutants in several genes, including *RSW1/CesA1*, *RSW5/CesA3*, *QUILL/PROCUSTE/CesA6*, *POM-POM1/CHITINASE LIKE1* (*POM1/CTL1*), *KORRIGAN/LION'S TAIL1/RADIALLY SWOLLEN2* (*KOR/LIT/RSW2*), *COBRA* and *KOBITO/ELONGATION DEFECTIVE1* (*KOB1/ELD1*), involved in cellulose biosynthesis or cell wall modification were reported to have cell swelling and dwarfing phenotypes similar to that observed in 35S::AtDICE1 plants (Hauser *et al.*, 1995; Arioli *et al.*, 1998; Nicol *et al.*, 1998; Fagard *et al.*, 2000; Lane *et al.*, 2001; Schindelman *et al.*, 2001; Pagant *et al.*, 2002; Wang *et al.*, 2006). The *korrigan* mutant showed abnormal cell expansion phenotypes in roots and hypocotyls, and was found to be defective in an endo-1,4-D-glucanase (Nicol *et al.*, 1998). The *cobra* mutant exhibited abnormal cell expansion and cellulose deposition in root cells resulting from a failure of orientated cell expansion (Roudier *et al.*, 2002).

Furthermore, our whole transcriptome analysis revealed the relevant transcription profile of 35S::AtDICE1 plants responsible for the defects in anisotropic cell expansion (Table 1). For example, expression of the *MYB21* and *ANAC036* transcription factors, which are known to negatively regulate cell elongation, were up-regulated up to 7.9-fold in 35S::AtDICE1 plants. Overexpression of an MYB21-GR fusion protein resulted in decreased hypocotyl cell expansion, shorter stems, and smaller and narrower leaves (Shin *et al.*, 2002). Overexpression of ANAC036 also resulted in a semi-dwarf phenotype (Kato *et al.*, 2010). In addition, many cell wall formation/modification-related genes were upregulated, including xyloglucan endotransglucosylase/hydrolase (XTH22/TCH4 and XTH23), pectinesterase, cellulose synthase-like A01, lipid transfer proteins and peroxidase (Passardi *et al.*, 2004; Nieuwland *et al.*, 2005) (Table 1).

Upregulation of AtDICE1 invokes a cellular defence mechanism

Interference with cell wall integrity results in various compensatory reactions, such as the reactive oxygen species (ROS) response, ectopic lignin deposition (Caño-Delgado *et al.*, 2003; Denness *et al.*, 2011), altered pectin methyl-esterification status (Manfield *et al.*, 2004), elevated callose deposition (Desprez

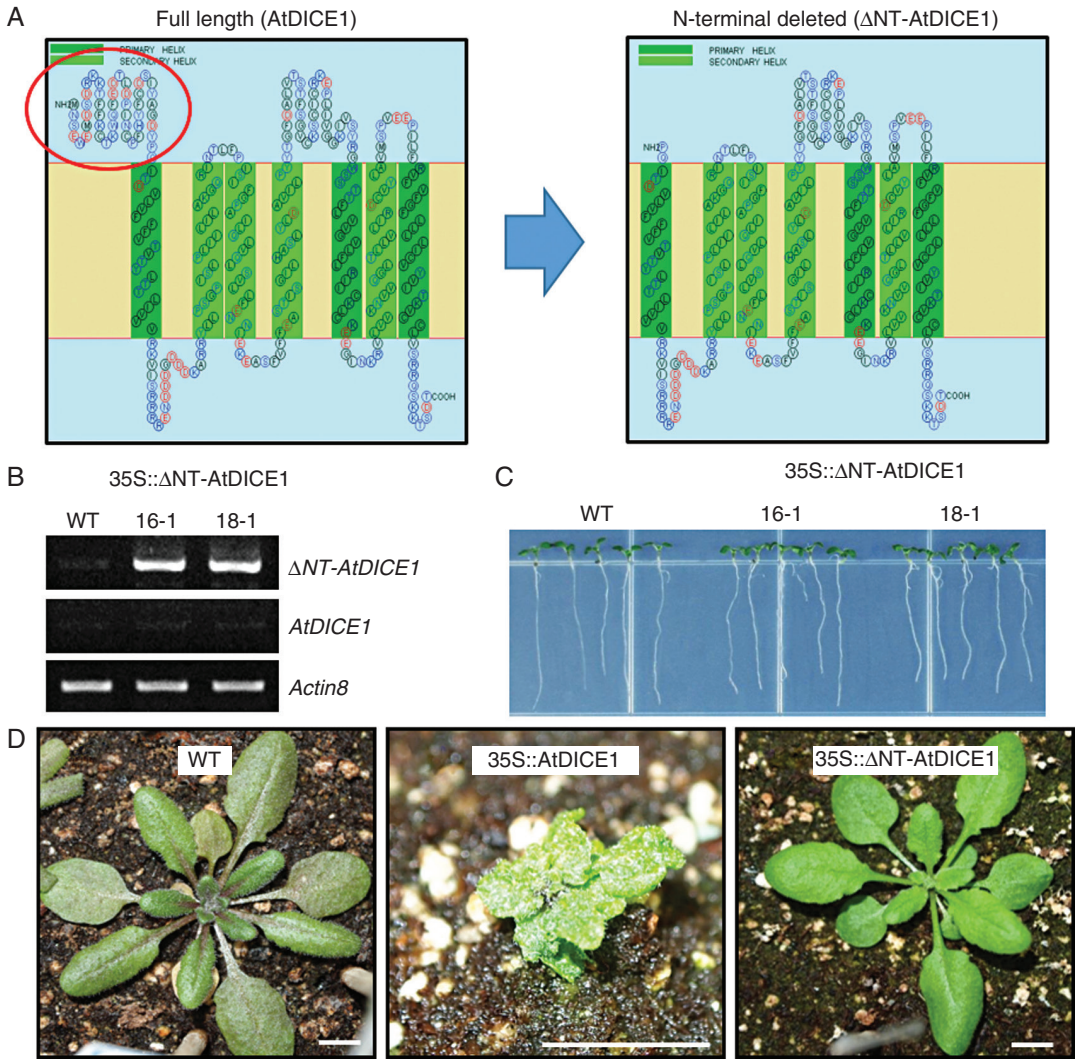

FIG. 6. The N-terminal conserved domain is necessary for AtDICE1 function. (A) Schematic diagram of full length (left) and N-terminal conserved domain-deleted (right; ΔNT-AtDICE1) AtDICE1. The N-terminal conserved domain is indicated by the red circle. (B) Semi-quantitative RT-PCR analysis to confirm the expression of Δ*NT-AtDICE1* in 35S::ΔNT-AtDICE1 plants. (C) Seven-day-old 35S::ΔNT-AtDICE1 seedlings compared to WT. (D) Phenotypic consequences in a 33-d-old 35S::ΔNT-AtDICE1 plant compared to both WT and 35S::AtDICE1 plants. Scale bars indicate 1 cm.

et al., 2002), and increased JA and ethylene production with an associated resistance to pathogens (Ellis *et al.*, 2002). Thus, the finding that a high proportion (51.4 %) of the upregulated genes in 35S::AtDICE1 plants were genes involved in stress and defence responses can be explained as the response of plant cells to changes in cell wall integrity and abnormal cell shape (Fig. 7 and Table 1). In particular, JA biosynthesis, signalling and responsive genes were massively upregulated. For example, *Thionin 2.1* (AT1G72260), a cysteine-rich protein with anti-microbial properties, was dramatically upregulated (up to 1185-fold). Myrosinase-binding proteins (MBP1, AT1G52040; and MBP2, AT1G52030), involved in metabolizing defence compounds to protect against herbivory, were upregulated (up to 18-fold). Additionally, vegetative storage proteins (VSP1, AT5G24780; and VSP2, AT5G24770), known to be induced by JA, were upregulated (up to six-fold).

It has been reported that COBRA, a glycosyl phosphatidyl inositol (GPI)-anchored protein, is targeted to the plasma membrane and involved in orientated cell expansion in Arabidopsis (Roudier *et al.*, 2005). *cob-5*, a loss-of-function mutant of *COBRA* with an epidermal cell swelling phenotype similar to 35S::AtDICE1, over-accumulates JA and coordinately induces stress- and defence-related genes (Ko *et al.*, 2006*b*). Interestingly, our whole transcriptome analysis revealed that the upregulated genes in 35S::AtDICE1 plants overlapped dramatically with those upregulated in *cob-5*. Specifically, 32 of the 72 upregulated genes were also upregulated more than three-fold in *cob-5* and, among them (i.e. 32 genes), 23 genes (~72 %) were involved in the stress/defence response (Table 1). This suggests that the changes in cell wall integrity caused by cell swelling in 35S::AtDICE1 plants induce cellular defence responses as in *cob-5*. Taken together, these results further support the hypothesis that plant cells initially perceive biotic stress at the cell surface (Ko *et al.*, 2006*b*).

While the overexpression of *AtDICE1* induced conspicuous phenotypes, the suppression of *AtDICE1* resulted in no

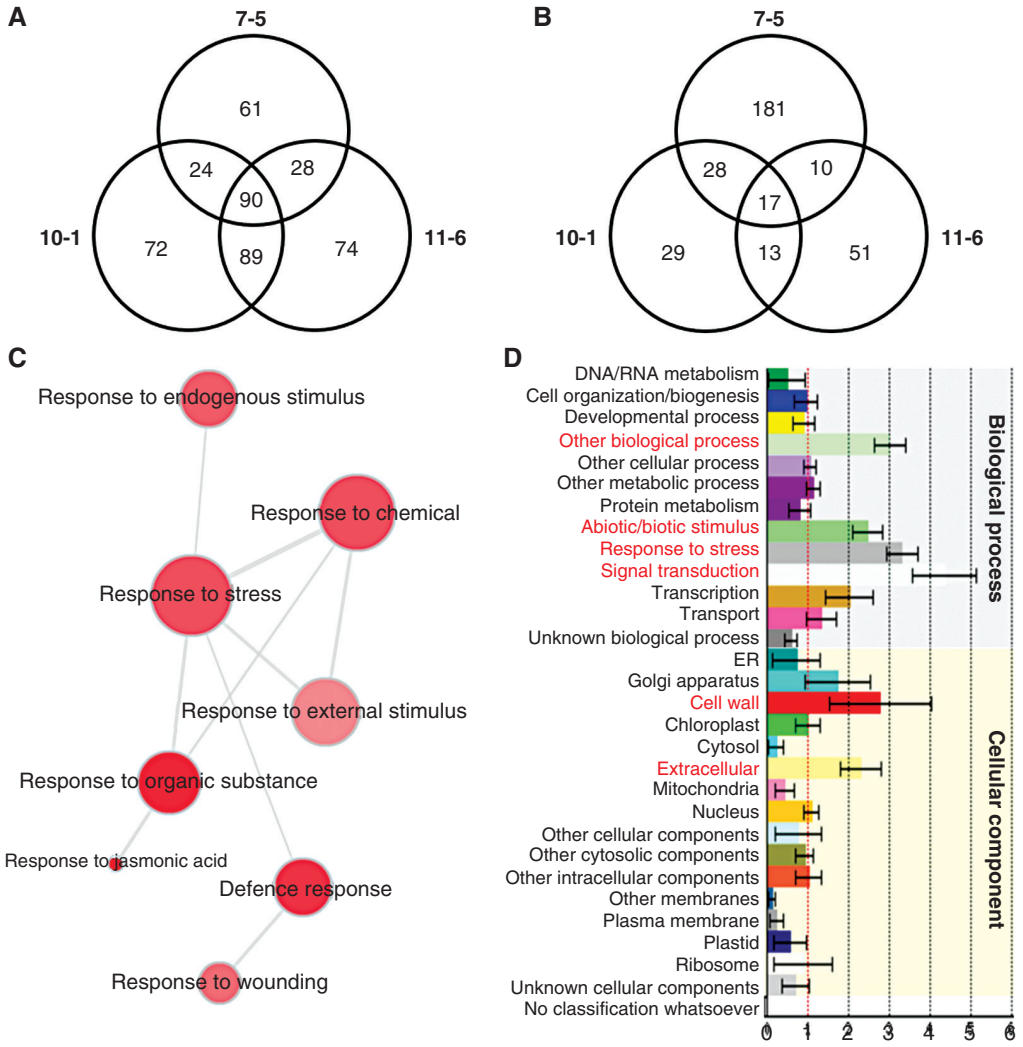

FIG. 7. Whole transcriptome analyses of 7-d-old 35S::AtDICE1 plants compared to WT. (A and B) Venn diagrams showing differentially expressed probe sets from three independent lines (i.e. 7-5, 10-1, 11-6) of 35S::AtDICE1 plants compared to WT. The number of probe sets in each line is displayed within a circle. The number of common probe sets is shown in the intersections between lines. Upregulated (A) or downregulated (B) probe sets in each line compared to WT using a three3-fold change as the threshold. (C) Gene Ontology (GO) analysis performed using REVIGO (http://revigo.irb.hr/). The representative GO terms of the 90 upregulated probe sets of A are visualized in semantic similarity-based scatterplots. (D) Functional classification generated using the Classification SuperViewer (http://bar.utoronto.ca/ntools/cgi-bin/ntools_classification_superviewer.cgi). The Classification SuperViewer generates an overview of functional classification of the 90 upregulated probe sets of A based on the GO database. The input set was bootstrapped 100 times to provide an idea as to over- or underrepresentation reliability. Gene categories are shown on the left, and their normalized frequencies are found on the *x*-axis and are calculated as follows: (Number_in_Classinput_set/Number_Classifiedinput_set)/(Number_in_Classreference_set (25k)/Number_Classifiedreference_set).

distinguishable phenotypic changes compared to WT (Fig. S4). However, expression of *Thionin 2.1*, which was dramatically upregulated in 35S::AtDICE1 plants, was significantly downregulated in AtDICE1_RNAi plants (Fig. S6). Thus, it is possible that the suppression of *AtDICE1* in AtDICE1_RNAi plants was not strong enough to cause phenotypic changes. Generating a loss-of-function mutant using CRISPR/Cas9 technology may be required to address this hypothesis.

Functional significances of AtDICE1

Amino acid sequence analysis predicted that AtDICE1 is a membrane protein having seven transmembrane domains, and containing a putative di-lysine (KK) motif at the C-terminus, which is required for ER targeting (Fig. S2; Teasdale and Jackson, 1996). Indeed, the results of our transient expression analysis of GFP:AtDICE1 suggest that AtDICE1 is probably localized to the ER (Fig. 5). The ER is a cytoplasmic network of flattened, membrane-enclosed sacs or tube-like structures known as cisternae that play important roles in the folding of protein molecules and the transport of synthesized proteins in vesicles to the Golgi apparatus (Chen *et al.*, 2012). Correct folding of newly synthesized proteins is made possible by several ER chaperone proteins and only properly folded proteins are transported from the rough ER to the Golgi apparatus. We hypothesize that AtDICE1 might be involved in the processing of some proteins responsible for cell wall formation, such

TABLE 1. *List of genes upregulated in 35S::AtDICE1 plants*

AGI*	WT	F†	7-5	F	10-1	F	11-6	F	7-5/WT‡	10-1/ WT	11-6/ WT	cob-5 / WT§	Gene description	St/Def¶
AT1G72260	6.7	A	7978.0	P	2015.0	P	2907.6	P	1185.5	299.3	431.9	106.4	thionin 2.1	YES
AT4G15100	15.9	A	1239.8	P	156.3	P	88.0	P	78.2	9.9	5.5	12.5	serine carboxypeptidase-like 30	
AT2G39330	267.0	P	8145.8	P	4897.3	P	4446.0	P	30.5	18.3	16.7	43.1	jacalin-related lectin 23	YES
AT2G41610	408.1	P	8791.5	P	6760.8	P	3807.9	P	21.5	16.6	9.3	0.7	AtDCE1	
AT1G54020	166.3	P	3426.4	P	1788.4	P	1949.7	P	20.6	10.8	11.7	53.9	GDSL esterase/lipase	YES
AT1G52030	805.8	P	14800.8	P	9016.5	P	10847.8	P	18.4	11.2	13.5	n/a	myrosinase-binding protein 2	YES
AT1G52040	181.9	P	2666.8	P	2117.9	P	2019.6	P	14.7	11.6	11.1	27.6	myrosinase-binding protein 1	YES
AT1G33760	41.1	P	525.4	P	394.8	P	295.1	P	12.8	9.6	7.2	20.2	ERF022	YES
AT4G01985	16.9	A	215.6	P	298.5	P	118.7	P	12.7	17.6	7.0	n/a	hypothetical protein	
AT3G28220	3471.2	P	38 894.9	P	28 177.1	P	36 552.9	P	11.2	8.1	10.5	13.6	TRAF-like family protein	
AT1G66370	43.3	P	478.5	P	254.8	P	224.4	P	11.1	5.9	5.2	7.4	MYB113	YES
AT4G27160	17.4	A	167.7	P	53.5	P	162.2	P	9.6	3.1	9.3	0.3	seed storage albumin 3	
AT1G35140	1734.1	P	15 869.4	P	13 207.7	P	17 206.2	P	9.2	7.6	9.9	3.5	PHI-1/EXL1	YES
AT5G28237	4.9	A	41.3	P	51.1	P	26.7	P	8.4	10.3	5.4	n/a	tryptophan synthase-like protein	
AT4G27170	18.9	A	157.0	P	57.5	P	103.7	P	8.3	3.0	5.5	0.5	seed storage albumin 4	
AT3G27810	7.2	A	53.6	P	57.1	P	45.0	P	7.4	7.9	6.2	1.6	MYB21	YES
AT4G17920	25.1	A	184.6	P	247.3	P	222.6	P	7.3	9.8	8.9	n/a	RING-H2 finger protein ATL29	
AT1G61120	21.4	A	150.9	P	180.1	P	321.5	P	7.0	8.4	15.0	71.5	terpene synthase 04	YES
AT1G17380	222.5	P	1471.2	P	982.5	P	1118.6	P	6.6	4.4	5.0	21.7	JAZ5/TIFY 11A	YES
AT4G34410	35.5	P	230.8	P	121.3	P	148.0	P	6.5	3.4	4.2	0.3	ERF109	YES
AT1G52400	11461.6	P	72 721.5	P	44 118.3	P	51 794.5	P	6.3	3.8	4.5	3.1	BGLU18/beta glucosidase 18	YES
AT1G52410	3933.8	P	23 332.2	P	16 344.8	P	15 134.4	P	5.9	4.2	3.8	21.9	TSK-associating protein 1	YES
AT3G25180	11.3	A	66.3	P	70.7	P	131.2	P	5.9	6.3	11.7	2.9	CYP82G1	YES
AT1G76640	174.4	P	999.9	P	660.1	P	551.5	P	5.7	3.8	3.2	19.2	calcium-binding protein CML39	
AT2G34600	244.6	P	1319.1	P	798.1	P	1062.2	P	5.4	3.3	4.3	1.7	JAZ7/TIFY 5B	YES
AT5G41750	622.9	P	3355.5	P	2809.3	P	2847.5	P	5.4	4.5	4.6	n/a	TIR-NBS-LRR disease-resistant protein	YES
AT5G59310	1746.9	P	9175.7	P	24 203.0	P	17 251.5	P	5.3	13.9	9.9	1.7	non-specific lipid-transfer protein 4	YES
AT5G41740	354.1	P	1794.6	P	1501.2	P	1671.3	P	5.1	4.2	4.7	4.7	TIR-NBS-LRR disease-resistant protein	YES
AT1G66610	16.7	A	83.5	P	91.2	P	54.5	P	5.0	5.4	3.3	1.5	E3 ubiquitin-ligase SINA-like 1	
AT1G66860	6.8	A	33.6	P	48.6	P	30.9	P	5.0	7.2	4.6	2.6	Class I glutamine amidotransferase-like	
AT4G28790	21.5	A	100.4	P	172.9	P	175.4	P	4.7	8.1	8.2	n/a	transcription factor bHLH23	
AT5G59580	17.2	A	77.4	P	66.9	P	66.7	P	4.5	3.9	3.9	0.8	UDP-glucosyl transferase 76E1/UGT76E1	
AT5G24780	7476.2	P	33 245.3	P	35 412.6	P	39 064.4	P	4.4	4.7	5.2	4.8	vegetative storage protein 1	YES
AT4G11911	15.3	A	67.4	P	132.8	P	84.5	P	4.4	8.7	5.5	n/a	hypothetical protein	
AT5G13220	260.0	P	1124.2	P	815.6	P	886.6	P	4.3	3.1	3.4	11.0	JAZ10/TIFY 9	YES
AT1G77640	338.2	P	1433.9	P	1595.4	P	1283.1	P	4.2	4.7	3.8	2.4	ERF013	
AT3G27415	20.9	A	87.1	P	146.4	P	111.3	P	4.2	7.0	5.3	n/a	hypothetical protein	
AT5G57560	5382.4	P	22 307.3	P	21 813.0	P	21 676.0	P	4.1	4.1	4.0	1.3	TCH4/XTH22	
AT4G23215	17.7	A	73.1	P	89.4	P	74.1	P	4.1	5.0	4.2	n/a	hypothetical protein	
AT4G29570	16.6	A	68.0	P	175.5	P	185.8	P	4.1	10.6	11.2	2.7	cytidine/deoxycytidylate deaminase-like	
AT2G32200	259.6	P	1056.0	P	838.7	P	1025.1	P	4.1	3.2	3.9	n/a	unknown protein	
AT1G03880	38.8	P	155.0	P	118.8	P	557.6	P	4.0	3.1	14.4	2.2	cruciferin 2	YES
AT4G10265	208.0	P	824.1	P	850.3	P	994.6	P	4.0	4.1	4.8	n/a	putative wound-responsive protein	YES
AT5G24770	10375.6	P	40 351.9	P	65 197.1	P	55 171.0	P	3.9	6.3	5.3	n/a	vegetative storage protein 2	YES
AT4G12735	11.8	A	45.1	P	40.4	P	41.3	P	3.8	3.4	3.5	n/a	hypothetical protein	
AT5G30341	9.5	A	36.2	P	43.5	P	40.7	P	3.8	4.6	4.3	n/a	hypothetical protein	
AT5G11410	447.9	P	1698.6	P	1865.2	P	1458.5	P	3.8	4.2	3.3	18.9	protein kinase family protein	
AT1G52000	482.5	P	1782.7	P	1549.3	P	1480.3	P	3.7	3.2	3.1	7.1	jacalin-like lectin domain protein	YES
AT4G16590	33.7	P	124.4	P	247.1	P	397.6	P	3.7	7.3	11.8	4.2	cellulose synthase-like A01	
AT5G52760	107.3	P	395.5	P	503.6	P	354.6	P	3.7	4.7	3.3	7.9	copper transport family protein	
AT1G21910	2375.9	P	8713.1	P	7190.5	P	7939.6	P	3.7	3.0	3.3	2.5	ERF012/DREB26	YES
AT5G58400	52.8	P	193.5	P	184.9	P	170.7	P	3.7	3.5	3.2	1.2	peroxidase 68	YES
AT1G69880	1654.5	P	6054.5	P	6756.3	P	6254.5	P	3.7	4.1	3.8	11.6	thioredoxin H8	YES

(continued)

TABLE 1. *Continued*

AGI*	WT	F†	7-5	F	10-1	F	11-6	F	7-5/WT‡	10-1/ WT	11-6/ WT	cob-5 / WT§	Gene description	St/Def¶
AT1G19610	305.4	P	1104.3	P	1089.4	P	1019.9	P	3.6	3.6	3.3	9.3	PDF1.4/defensin-like protein 19	YES
AT2G38250	121.0	P	435.5	P	681.0	P	363.1	P	3.6	5.6	3.0	3.6	DNA-binding protein	
AT5G49520	284.6	P	998.3	P	991.5	P	900.4	P	3.5	3.5	3.2	3.7	WRKY48	YES
AT3G57260	74.7	P	260.4	P	800.4	P	1107.0	P	3.5	10.7	14.8	8.4	BGL2/β-1,3-glucanase 2/PR2	YES
AT1G68290	172.0	P	599.1	P	532.4	P	625.9	P	3.5	3.1	3.6	2.4	endonuclease 2	
AT2G17040	1983.1	P	6898.2	P	6486.4	P	5957.2	P	3.5	3.3	3.0	5.0	ANAC036	YES
AT4G02170	45.9	P	157.5	P	188.2	P	172.0	P	3.4	4.1	3.7	2.3	hypothetical protein	
AT4G02330	4488.5	P	15 318.2	P	18 712.9	P	21 081.7	P	3.4	4.2	4.7	10.0	pectinesterase/ATPMEPCRB	
AT3G50770	504.3	P	1692.4	P	1544.9	P	2176.5	P	3.4	3.1	4.3	2.1	calcium-binding protein CML41	
AT1G72520	438.8	P	1431.8	P	1316.7	P	2118.1	P	3.3	3.0	4.8	8.2	lipoxygenase 4	YES
AT2G35290	468.8	P	1491.9	P	1571.7	P	1476.1	P	3.2	3.4	3.1	0.8	SAUR79	
AT3G02550	111.9	P	351.8	P	411.3	P	461.1	P	3.1	3.7	4.1	1.2	LOB41	YES
AT4G32060	15.2	A	47.6	P	54.6	P	86.8	P	3.1	3.6	5.7	0.7	calcium-binding EF hand protein	
AT4G25810	2394.0	P	7487.3	P	8327.9	P	7563.7	P	3.1	3.5	3.2	5.2	XTH23	
AT1G63750	1816.6	P	5667.8	P	6791.9	P	7526.2	P	3.1	3.7	4.1	1.7	TIR-NBS-LRR disease-resistant protein	YES
AT2G14560	72.0	P	222.7	P	521.3	P	253.2	P	3.1	7.2	3.5	3.8	LURP1	YES
AT2G05580	32.8	P	100.1	P	130.3	P	115.9	P	3.1	4.0	3.5	0.2	glycine-rich protein	
AT4G14365	591.9	P	1784.3	P	2416.5	P	2205.6	P	3.0	4.1	3.7	4.9	E3 ubiquitin-protein ligase XBAT34	YES
AT2G23100	19.5	A	58.7	P	61.5	P	87.2	P	3.0	3.2	4.5	1.5	cys/his-rich C1 domain protein	

*AGI, Arabidopsis Gene Index.

†F, flag calling (presence, absence, marginal).

‡Fold change.

§Data from Ko *et al.* (2006*b*).

¶Stress/defence-related genes.

as CesA proteins, in the ER via a currently unknown mechanism. Previously, mutants of the *PEANUT1* gene encoding an ER-localized mannosyltransferase required for synthesis of the GPI anchor showed radially swollen embryos and decreased crystalline cellulose in the cell wall (Gillmor *et al.*, 2005). Thus, it might also be plausible that the overly increased AtDICE1 protein population in the ER might disturb other proteins such as PEANUT1. If this is the case, the N-terminal external domain is obligatory because overexpression of ΔNT-AtDICE1 was not associated with any phenotypic changes (Fig. 6). In addition, because AtDICE1 was identified as a member of a gene network regulating secondary xylem development in Arabidopsis (Ko *et al.*, 2006*a*) and confirmed to be expressed specifically in vascular tissues (Fig. S1), it might be plausible that AtDICE1 may function in vascular tissue formation by regulating anisotropic cell elongation.

It remains uncertain how cell elongation is integrated with secondary wall formation, which occurs irreversibly in some specialized cells such as xylem cells and fibres after cessation of cell elongation (Boerjan *et al.*, 2003; Déjardin *et al.*, 2010). Previously, the *eli1* mutant exhibited a stunted phenotype and xylem cell disorganization in stem pith, which was caused by altered cell expansion with inappropriate initiation of secondary wall formation (Caño-Delgado *et al.*, 2000). Because ectopic secondary wall formation or lignification phenotypes were observed in many other cell expansion mutants (e.g. *rsw1*, *korrigan1*/*lit*, *det3*), a mechanism that senses cell size and induces subsequent secondary wall formation may exist (Caño-Delgado *et al.*, 2000). Subsequently, it was shown that *eli1* mutants occur in the cellulose synthase gene *CesA3* (Caño-Delgado *et al.*, 2003). Recently, AtC3H14, a plant-specific tandem CCCH zinc-finger protein, was suggested to be a coordinate regulator of cell elongation and secondary wall formation during xylogenesis because overexpression of *AtC3H14* or *PtC3H17*, a poplar homologuw of *AtC3H14*, suppressed cell elongation but increased secondary wall thickening (Kim *et al.*, 2014; Chai *et al.*, 2015). In this report, we found abnormal secondary wall thickenings in the pith cells of 35S::AtDICE1 and 35S::PtrDICE1 plants (Figs 8 and S7). This result further supports the hypothesis that a cell size sensing mechanism exists, leading to secondary wall formation. However, because these abnormal secondary wall thickenings in stem tissues of 35S::AtDICE1 plant are patchy (Fig. S7B), we assumed that the overall cellulose contents in adult stems of 35S::AtDICE1 plants were lower than in the WT, as shown in Fig. 4B. Furthermore, expression of *AtC3H14* was not significantly altered in 35S::AtDICE1 plants and, furthermore, no changes in *AtDICE1* were observed in 35S::AtC3H14 plants (data not shown), suggesting that it is unlikely that a mechanistic connection exists between them.

In conclusion, our data suggest that AtDICE1 is a novel putative ER-localized transmembrane protein contributing to a proper anisotropic cell elongation process through participation in cell wall formation via a currently unknown mechanism. Because AtDICE1 was identified as a member of a gene network regulating secondary xylem development in Arabidopsis (Ko *et al.*, 2006*a*) and confirmed to be expressed specifically

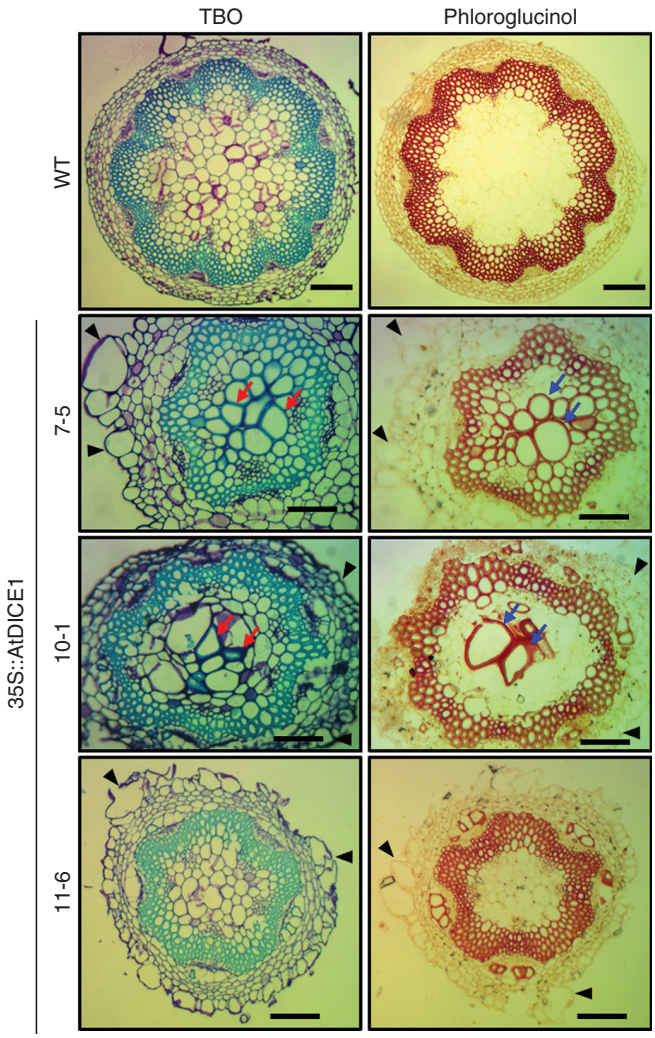

FIG. 8. 35S::AtDICE1 plants showed abnormal secondary wall thickenings in pith of inflorescent stems. Stem cross-sections of 50-d-old 35S::AtDICE1 and WT plants stained with 0.05 % toluidine blue *O* (TBO) and 2 % phloroglucinol/HCl (Phloroglucinol) as indicated. Pith cells having secondary wall thickenings are indicated by arrows and swollen cells by arrowheads. Scale bars represent 100 µm.

in secondary wall-forming tissues (Fig. S1), it is possible that AtDICE1 might be involved in the anisotropic cell elongation during xylogenesis. Further in-depth investigations, including loss-of-function mutation employing CRISPR/Cas9 technology, immunohistochemistry and protein–protein interactions with cell-wall-forming proteins (e.g. AtDICE1 with CESA complexes), will be required to elucidate AtDICE1 function in detail.

SUPPLEMENTARY DATA

Supplementary data are available online at https://academic.oup.com/aob and consist of the following. Table S1: Growth features of 35S::AtDICE1. Table S2: List of genes differentially expressed in 35S::AtDICE1. Table S3: Primers used in this study. Figure S1: *AtDICE1* (At2g41610) is specifically expressed in vascular tissues/cells. Figure S2: AtDICE1 is a plant-specific transmembrane protein. Figure S3: Floral organs of 35S::AtDICE1 plants are smaller than in WT. Figure S4: Phenotypic characterization of AtDICE1_RNAi plants. Figure S5: Confirmation of the microarray data using semi-quantitative RT-PCR analysis. Figure S6: Expression of the *Thionin 2.1* gene was significantly downregulated in AtDICE1_RNAi plants. Figure S7: 35S::PtrDICE1 resulted in abnormal secondary wall thickenings in pith cells as in 35S::AtDICE1 plants.

ACKNOWLEDGEMENTS

We are grateful to Prof. Kim (Youngrok) at Kyung Hee University for technical assistance with SEM analysis. This work was supported by the Forest Resources Genome Project (2014071G10-1722-AA04) and by a grant from the Basic Science Research Program through the National Research Foundation of Korea (NRF-2015R1D1A1A01060807).

LITERATURE CITED

Arioli T, **Peng L**, **Betzner AS**, ***et al.* 1998**. Molecular analysis of cellulose biosynthesis in Arabidopsis. *Science* **279**: 717–720.

Baskin TI. 2005. Anisotropic expansion of the plant cell wall. *Annual Review of Cell and Developmental Biology* **21**: 203–222.

Boerjan W, **Ralph J**, **Baucher M. 2003**. Lignin biosynthesis. *Annual Review of Plant Biology* **54**: 519–546.

Bringmann M, **Li E**, **Sampathkumar A**, **Kocabek T**, **Hauser MT**, **Persson S. 2012**. POM-POM2/CELLULOSE SYNTHASE INTERACTING1 is essential for the functional association of cellulose synthase and microtubules in Arabidopsis. *Plant Cell* **24**: 163–177.

Caño-Delgado AI, **Metzlaff K**, **Bevan MW. 2000**. The *eli1* mutation reveals a link between cell expansion and secondary cell wall formation in *Arabidopsis thaliana*. *Development* **127**: 3395–3405.

Caño-Delgado AI, **Penfield S**, **Smith C**, **Catley M**, **Bevan M. 2003**. Reduced cellulose synthesis invokes lignification and defense responses in *Arabidopsis thaliana*. *The Plant Journal* **34**: 351–362.

Carpita NC. 2011. Update on mechanisms of plant cell wall biosynthesis: how plants make cellulose and other (1→4)-β-d-glycans. *Plant Physiology* **155**: 171–184.

Chai G, **Kong Y**, **Zhu M**, ***et al.* 2015**. Arabidopsis C3H14 and C3H15 have overlapping roles in the regulation of secondary wall thickening and anther development. *Journal of Experimental Botany* **66**: 2595–2609.

Chen J, **Doyle C**, **Qi X**, **Zheng H. 2012**. The endoplasmic reticulum: a social network in plant cells. *Journal of Integrative Plant Biology* **54**: 840–850.

Clough SJ, **Bent AF. 1998**. Floral dip: a simplified method for *Agrobacterium*-mediated transformation of *Arabidopsis thaliana*. *The Plant Journal* **16**: 735–743.

Cosgrove DJ. 2005. Growth of the plant cell wall. *Nature Reviews Molecular Cell Biology* **6**: 850–861.

Curtis MD, **Grossniklaus U. 2003**. A gateway cloning vector set for high-throughput functional analysis of genes in planta. *Plant Physiology* **133**: 462–469.

Déjardin A, **Laurans F**, **Arnaud D**, **Breton C**, **Pilate G**, **Leplé JC. 2010**. Wood formation in Angiosperms. *Comptes Rendus Biologies* **333**: 325–334.

Denness L, **McKenna JF**, **Segonzac C**, ***et al.* 2011**. Cell wall damage-induced lignin biosynthesis is regulated by a reactive oxygen species- and jasmonic acid-dependent process in Arabidopsis. *Plant Physiology* **156**: 1364–1374.

Desprez T, **Vernhettes S**, **Fagard M**, ***et al.* 2002**. Resistance against herbicide isoxaben and cellulose deficiency caused by distinct mutations in same cellulose synthase isoform CESA6. *Plant Physiology* **128**: 482–490.

Di Sansebastiano GP, **Renna L**, **Piro G**, **Dalessandro G. 2004**. Stubborn GFPs in *Nicotiana tabacum* vacuoles. *Plant Biosystems* **138**: 37–42.

Ellis C, **Turner JG. 2001**. The Arabidopsis mutant *cev1* has constitutively active jasmonate and ethylene signal pathways and enhanced resistance to pathogens. *Plant Cell* **13**: 1025–1033.

Ellis C, **Karafyllidis I**, **Wasternack C**, **Turner JG. 2002**. The Arabidopsis mutant *cev1* links cell wall signaling to jasmonate and ethylene responses. *Plant Cell* **14**: 1557–1566.

Endler A, **Kesten C**, **Schneider R**, ***et al.* 2015**. A mechanism for sustained cellulose synthesis during salt stress. *Cell* **162**: 1353–1364.

Fagard M, **Desnos T**, **Desprez T**, ***et al.* 2000**. PROCUSTE1 encodes a cellulose synthase required for normal cell elongation specifically in roots and dark-grown hypocotyls of Arabidopsis. *Plant Cell* **12**: 2409–2424.

Geisler DA, **Sampathkumar A**, **Mutwil M**, **Persson S. 2008**. Laying down the bricks: logistic aspects of cell wall biosynthesis. *Current Opinion in Plant Biology* **11**: 647–652.

Gibeaut DM, **Carpita NC. 1994**. Biosynthesis of plant cell wall polysaccharides. *The FASEB Journal* **8**: 904–915.

Gillmor CS, **Lukowitz W**, **Brininstool G**, ***et al.* 2005**. Glycosylphosphatidylinositol-anchored proteins are required for cell wall synthesis and morphogenesis in Arabidopsis. *Plant Cell* **17**: 1128–1140.

Green PB. 1962. Mechanism for plant cellular morphogenesis. *Science* **138**: 1404–1405.

Gutierrez R, **Lindeboom JJ**, **Paredez AR**, **Emons AMC**, **Ehrhardt DW. 2009**. Arabidopsis cortical microtubules position cellulose synthase delivery to the plasma membrane and interact with cellulose synthase trafficking compartments. *Nature Cell Biology* **11**: 797–806.

Hauser MT, **Morikami A**, **Benfey PN. 1995**. Conditional root expansion mutants of Arabidopsis. *Development* **121**: 1237–1252.

Hoebler C, **Barry JL**, **David A**, **Delort-Laval J. 1989**. Rapid acid hydrolysis of plant cell wall polysaccharides and simplified quantitative determination of their neutral monosaccharides by gas-liquid chromatography. *Journal of Agricultural and Food Chemistry* **37**: 360–367.

Höfgen R, **Willmitzer L. 1988**. Storage of competent cells for Agrobacterium transformation. *Nucleic Acids Research* **16**: 9877.

Jefferson RA, **Kavanagh TA**, **Bevan MW. 1987**. GUS fusions: beta-glucuronidase as a sensitive and versatile gene fusion marker in higher plants. *The EMBO Journal* **6**: 3901–3907.

Karimi M, **Inzé D**, **Depicker A. 2002**. GATEWAY vectors for *Agrobacterium*-mediated plant transformation. *Trends in Plant Science* **7**: 193–195.

Kato H, **Motomura T**, **Komeda Y**, **Saito T**, **Kato A. 2010**. Overexpression of the NAC transcription factor family gene ANAC036 results in a dwarf phenotype in *Arabidopsis thaliana*. *Journal of Plant Physiology* **167**: 571–577.

Kim WC, **Kim JY**, **Ko JH**, **Kang H**, **Kim J**, **Han KH. 2014**. AtC3H14, a plant-specific tandem CCCH zinc-finger protein, binds to its target mRNAs in a sequence-specific manner and affects cell elongation in *Arabidopsis thaliana*. *The Plant Journal* **80**: 772–784.

Ko JH, **Beers EP**, **Han KH. 2006*a***. Global comparative transcriptome analysis identifies gene network regulating secondary xylem development in *Arabidopsis thaliana*. *Molecular Genetics and Genomics* **276**: 517–531.

Ko JH, **Kim JH**, **Jayanty SS**, **Howe GA**, **Han KH. 2006*b***. Loss of function of COBRA, a determinant of oriented cell expansion, invokes cellular defence responses in *Arabidopsis thaliana*. *Journal of Experimental Botany* **57**: 2923–2936.

Lane DR, **Wiedemeier A**, **Peng L**, ***et al.* 2001**. Temperature-sensitive alleles of RSW2 link the KORRIGAN endo-1,4-beta-glucanase to cellulose synthesis and cytokinesis in Arabidopsis. *Plant Physiology* **126**: 278–288.

Lei L, **Li S**, **Bashline L**, **Gu Y. 2014**. Dissecting the molecular mechanism underlying the intimate relationship between cellulose microfibrils and cortical microtubules. *Frontiers in Plant Science* **5**: 90.

Li S, **Lei L**, **Somerville CR**, **Gu Y. 2012**. Cellulose synthase interactive protein 1 (CSI1) links microtubules and cellulose synthase complexes. *Proceedings of the National Academy of Sciences USA* **109**: 185–190.

Lloyd C, **Chan J. 2006**. Not so divided: the common basis of plant and animal cell division. *Nature Reviews Molecular Cell Biology* **7**: 147–152.

Manfield IW, **Orfila C**, **McCartney L**, ***et al.* 2004**. Novel cell wall architecture of isoxaben-habituated Arabidopsis suspension-cultured cells: global transcript profiling and cellular analysis. *The Plant Journal* **40**: 260–275.

McFarlane HE, **Döring A**, **Persson S. 2014**. The cell biology of cellulose synthesis. *Annual Review of Plant Biology* **65**: 69–94.

Nguyen VP, **Cho JS**, **Choi YI**, **Lee SW**, **Han KH**, **Ko JH. 2016**. Evaluation of a novel promoter from *Populus trichocarpa* for mature xylem tissue specific gene delivery. *Plant Physiology and Biochemistry* **104**: 226–233.

Nicol F, **His I**, **Jauneau A**, **Vernhettes S**, **Canut H**, **Höfte H. 1998**. A plasma membrane-bound putative endo-1,4-β-d-glucanase is required for normal wall assembly and cell elongation in Arabidopsis. *The EMBO Journal* **17**: 5563–5576.

Nieuwland J, **Feron R**, **Huisman BA**, ***et al.* 2005**. Lipid transfer proteins enhance cell wall extension in tobacco. *Plant Cell* **17**: 2009–2019.

Pagant S, **Bichet A**, **Sugimoto K**, ***et al.* 2002**. KOBITO1 encodes a novel plasma membrane protein necessary for normal synthesis of cellulose during cell expansion in Arabidopsis. *Plant Cell* **14**: 2001–2013.

Paredez AR, **Somerville CR**, **Ehrhardt DW. 2006**. Visualization of cellulose synthase demonstrates functional association with microtubules. *Science* **312**: 1491–1495.

Passardi F, **Penel C**, **Dunand C. 2004**. Performing the paradoxical: how plant peroxidases modify the cell wall. *Trends in Plant Science* **9**: 534–540.

Roudier F, **Schindelman G**, **DeSalle R**, **Benfey PN. 2002**. The COBRA family of putative GPI-anchored proteins in Arabidopsis. A new fellowship in expansion. *Plant Physiology* **130**: 538–548.

Roudier F, **Fernandez AG**, **Fujita M**, ***et al.* 2005**. COBRA, an Arabidopsis extracellular glycosyl-phosphatidyl inositol-anchored protein, specifically controls highly anisotropic expansion through its involvement in cellulose microfibril orientation. *Plant Cell* **17**: 1749–1763.

Schindelman G, **Morikami A**, **Jung J**, ***et al.* 2001**. COBRA encodes a putative GPI-anchored protein, which is polarly localized and necessary for oriented cell expansion in Arabidopsis. *Genes & Development* **15**: 1115–1127.

Shin B, **Choi G**, **Yi H**, ***et al.* 2002**. AtMYB21, a gene encoding a flower-specific transcription factor, is regulated by COP1. *The Plant Journal for Cell and Molecular Biology* **30**: 23–32.

Somerville C. 2006. Cellulose synthesis in higher plants. *Annual Review of Cell and Developmental Biology* **22**: 53–78.

Somerville C, **Bauer S**, **Brininstool G**, ***et al.* 2004**. Toward a systems approach to understanding plant cell walls. *Science* **306**: 2206–2211.

Teasdale RD, **Jackson MR. 1996**. Signal-mediated sorting of membrane proteins between the endoplasmic reticulum and the golgi apparatus. *Annual Review of Cell and Developmental Biology* **12**: 27–54.

Ueda K, **Matsuyama T. 2000**. Rearrangement of cortical microtubules from transverse to oblique or longitudinal in living cells of transgenic *Arabidopsis thaliana*. *Protoplasma* **213**: 28–38.

Wang J, **Howles PA**, **Cork AH**, **Birch RJ**, **Williamson RE. 2006**. Chimeric proteins suggest that the catalytic and/or C-terminal domains give CesA1 and CesA3 access to their specific sites in the cellulose synthase of primary walls. *Plant Physiology* **142**: 685–695.

Wolf S, **Hématy K**, **Höfte H. 2012**. Growth control and cell wall signaling in plants. *Annual Review of Plant Biology* **63**: 381–407.

Xiang C, **Han P**, **Lutziger I**, **Wang K**, **Oliver DJ. 1999**. A mini binary vector series for plant transformation. *Plant Molecular Biology* **40**: 711–717.

Zhang Y, **Nikolovski N**, **Sorieul M**, ***et al.* 2016**. Golgi-localized STELLO proteins regulate the assembly and trafficking of cellulose synthase complexes in Arabidopsis. *Nature Communication* **7**: 11656.